Archives of Hydro-Engineering and Environmental Mechanics
Vol. 50 (2003), No. 4, pp. 359–379

A Non-Local Hypoplastic Constitutive Law to describe Shear Localisation in Granular Bodies

Jacek Tejchman

Gdańsk University of Technology, Faculty of Civil Engineering,
80-952 Gdańsk, ul. Narutowicza 11/12, Poland, e-mail: tejchmk@pg.gda.pl

(Received July 07, 2003; revised September 22, 2003)

Abstract

The paper presents a FE-analysis of shear localisation in granular bodies by a finite element method based on a hypoplastic constitutive law. The law can reproduce essential features of granular bodies depending on the void ratio, pressure level and deformation direction. To realistically simulate the formation of a spontaneous shear zone inside cohesionless sand during plane strain compression, a hypoplastic constitutive law was extended by non-local terms. The effects of initial void ratio, pressure level and a characteristic length on the thickness of an interior shear zone were shown. The numerical results were compared with corresponding laboratory tests.

Key words: characteristic length, finite element method, non-local model, plane strain compression, shear localisation

1. Introduction

Localisation of deformation in the form of narrow zones of intense shearing is a fundamental phenomenon in granular materials. It can develop in granular bodies during processes of flow or shift of objects with sharp edges against granular materials (Vardoulakis 1980, Yoshida et al 1994, Tatsuoka et al 1991, 1994, Desrues et al 1996, Yagi et al 1997). It can occur spontaneously inside granular materials or can be induced along walls of stiff structures at granular bodies (Uesugi et al 1988, Tejchman 1989, Hassan 1995). An understanding of the mechanism of the formation of shear zones is important since they act as a precursor to ultimate soil failure.

Classical FE-analyses of shear zones are not able to describe properly both the thickness of localisation zones and distances between them, since they suffer from a spurious mesh sensitivity (its size and alignment). The rate boundary value problem becomes ill-posed, i.e. the governing differential equations of motion change the type by losing ellipticity for static and hiperbolicity for dynamic

problems (Benallal et al 1987, de Borst et al 1992). Thus, the localisation is reduced to zero-volume zones. To overcome this drawback, classical constitutive models require an extension in the form of a characteristic length to regularise the rate boundary value problem and to take into account microscopic inhomogeneities triggering shear localisation (e.g. size and spacing of microdefects, grain size, fiber spacing). Different strategies can be used to include a characteristic length and to capture properly the post-failure regime (in quasi-static problems): polar models (Mühlhaus 1990, Sluys 1992, Tejchman and Wu 1993, Tejchman et al 1999, Tejchman 2002), non-local models (Eringen 1981, Bazant et al 1987, Bazant and Lin 1988, Brinkgreve 1994), strain gradient models (Zbib and Aifantis 1988, Sluys 1992, Chambon et al 2001), and models with an artificial viscosity (Neddleman 1988, Sluys 1992, Needleman and Tvergaard 1992, Belytschko et al 1994, Ehlers and Volk 1998).

In this paper, a spontaneous shear localisation in granular bodies was investigated with a finite element method based on a hypoplastic constitutive law extended by non-local terms. The FE-analysis was performed with enhanced hypoplastic models for a specimen of dry sand subject to plane strain compression under constant lateral pressure.

2. Hypoplasticity

Hypoplastic constitutive laws (Gudehus 1996, Bauer 1996, von Wolffersdorff 1996, Tejchman 1997) are an alternative to elasto-plastic formulations for continuum modelling of granular materials. They describe the evolution of effective stress components with the evolution of strain components by a differential equation including isotropic linear and non-linear tensorial functions according to the representation theorem by Wang (1970). In contrast to elasto-plastic models, the decomposition of deformation components into elastic and plastic parts, yield surface, plastic potential, flow rule and hardening rule are not needed. The hypoplastic models describe the behaviour of so-called simple grain skeletons which are characterised by the following properties (Gudehus 1996):

- the state is fully defined through the skeleton pressure and the void ratio (inherent anisotropy of contact forces between grains is not considered and vanishing principal stresses are not allowed),
- deformation of the skeleton is due to grain rearrangements (e.g. small deformations $< 10^{-5}$ due to the elastic behaviour of grain contacts are negligible),
- grains are permanent (abrasion and crushing are excluded in order to keep the granulometric properties unchanged),
- three various void ratios decreasing exponentially with pressure are distinguished (minimum, maximum and critical),

- the material manifests an asymptotic behaviour for monotonous and cyclic shearing or SOM-states for proportional compression,
- rate effects are negligible,
- physico-chemical effects (capillary and osmotic pressure) and cementation of grain contacts are not taken into account.

The hypoplastic constitutive laws are of the rate type. Due to the incremental non-linearity with the deformation rate, they are able describe both non-linear stress-strain and volumetric behaviour of granular bodies during shearing up to and after the peak with a single tensorial equation. They include also: barotropy (dependence on pressure level), pycnotropy (dependence on density), dependence on the direction of deformation rate, dilatancy and contractancy during shearing with constant pressure, increase and release of pressure during shearing with constant volume, and material softening during shearing of a dense material. They are apt to describe stationary states, i.e. states in which a grain aggregate can be continuously deformed at constant stress and constant volume under a certain rate of deformation. Although the hypoplastic models are developed without recourse to concepts of the theory of plasticity, failure surface, flow rule and plastic potential are obtained as natural outcomes (Wu and Niemunis 1996). The feature of the model is a simple formulation and procedure for determination of material parameters with standard laboratory experiments. The parameters are related to granulometric properties encompassing grain size distribution curve, shape, angularity and hardness of grains (Herle and Gudehus 1999). Owing to this, one set of material parameters is valid within a large range of pressures and densities.

Stress changes due to the deformation of a granular body can generally be expressed by

$$\overset{o}{\sigma}_{ij} = F(e, \sigma_{kl}, d_{kl}), \tag{1}$$

wherein the Jaumann stress rate tensor (objective stress rate tensor) is defined by

$$\overset{o}{\sigma}_{ij} = \overset{\bullet}{\sigma}_{ij} - w_{ik}\sigma_{kj} + \sigma_{ik}w_{kj}, \tag{2}$$

F in Eq. 1 represents an isotropic tensor-valued function of its arguments, σ_{ij} is the Cauchy skeleton (effective) stress tensor, e the void ratio and d_{kl} the rate of deformations tensor (stretching tensor). If the volume of grains remains constant (i.e. incompressible grains), the rate of the void ratio can be expressed by the evolution equation:

$$\overset{\bullet}{e} = (1+e)d_{kk}. \tag{3}$$

The rate of deformation tensor d_{ij} and the spin tensor w_{ij} are related to the material velocity v as follows:

$$d_{ij} = (v_{i,j} + v_{j,i})/2, \quad w_{ij} = (v_{i,j} - v_{j,i})/2, \quad ()_{,i} = \partial()/\partial x_i. \tag{4}$$

The condition of the incremental non-linearity (Bauer 1996) requires that the tensorial function F in Eq. 1 is not differentiable only for $d_{ij} = 0$. Such requirement results in the following equation, where the function F is decomposed into two parts

$$\overset{o}{\sigma}_{ij} = A(e, \sigma_{kl}, d_{kl}) + B(e, \sigma_{ij})||d_{kl}||. \tag{5}$$

The function A is linear in d_{kl}, while the function B is non-linear in d_{kl}. $||d_{kl}||$ denotes the Euclidian norm $\sqrt{d_{kl}d_{kl}}$. Both functions are positively homogeneous to the first degree in d_{kl}, i.e. $\sigma_{kl}(\lambda d_{kl}) = \lambda\sigma_{kl}d_{kl}$ for any scalar $\lambda > 0$. In this way, Eq. 5 becomes rate-independent. Because $\sigma_{kl}(+d_{kl}) \neq \sigma_{kl}(-d_{kl})$, the hypoplastic constitutive equation is incrementally non-linear, which allows for description of the inelastic behaviour. Limit states are characterised by vanishing stress rates. Thus, the limit state and the flow rule can be calculated from Eq. 5 and there is no need to introduce different functions for loading and unloading. As a limit case during monotonous shearing, the critical state concept is also taken into account for both simultaneously vanishing stress rates and volumetric deformation rate, and a constant void ratio ($\overset{o}{\sigma}_{ij} = 0, d_{kk} = 0, \overset{\bullet}{e} = 0$).

The following representation of the general constitutive equation (Eq. 6) is used (Gudehus 1996, Bauer 1996):

$$\overset{o}{\sigma}_{ij} = f_s \left[L_{ij}\left(\hat{\sigma}_{kl}, d_{kl}\right) + f_d N_{ij}\left(\hat{\sigma}_{ij}\right)\sqrt{d_{kl}d_{kl}} \right], \tag{6}$$

where the normalised stress tensor $\hat{\sigma}_{ij}$ is defined by

$$\hat{\sigma}_{ij} = \frac{\sigma_{ij}}{\sigma_{kk}}. \tag{7}$$

The scalar factors $f_s = f_s(e, \sigma_{kk})$ and $f_d = f_d(e, \sigma_{kk})$ take into account the influence of the density and pressure level on the stress. The stiffness factor f_s is proportional to the granulate hardness h_s and depends on the mean stress and void ratio:

$$f_s = \frac{h_s}{nh_i}\left(\frac{1+e_i}{e}\right)\left(-\frac{\sigma_{kk}}{h_s}\right)^{1-n} \tag{8}$$

with

$$h_i = \frac{1}{c_1^2} + \frac{1}{3} - \left(\frac{e_{i0} - e_{d0}}{e_{c0} - e_{d0}}\right)^{\alpha} \frac{1}{c_1\sqrt{3}}. \tag{9}$$

The granulate hardness represents h_s a density-independent reference pressure and is related to the entire skeleton (not to single grains). The density factor f_d resembles a pressure-dependent relative density index and is represented by

$$f_d = \left(\frac{e - e_d}{e_c - e_d}\right)^{\alpha}. \tag{10}$$

Here e is the current void ratio, e_c is the critical void ratio, e_d denotes the void ratio at maximum densification (due to cyclic shearing), e_i is the maximum void ratio, α denotes the pycnotropy coefficient, and n is the compression coefficient. The void ratio e is thus limited by e_i and e_d. The values of e_i, e_d and e_c are assumed to decrease with the pressure $-\sigma_{kk}$ according to the equations:

$$e_i = e_{i0} \exp\left[-(-\sigma_{kk}/h_s)^n\right], \tag{11}$$

$$e_d = e_{d0} \exp\left[-(-\sigma_{kk}/h_s)^n\right], \tag{12}$$

$$e_c = e_{c0} \exp\left[-(-\sigma_{kk}/h_s)^n\right], \tag{13}$$

wherein e_{i0}, e_{d0} and e_{c0} are the values of e_i, e_d and e_c for $\sigma_{kk} = 0$, respectively. For the tensorial functions L_{ij} and N_{ij}, the following representatives are used (Gudehus 1996, Bauer 1996, Tejchman 1997):

$$L_{ij} = a_1^2 d_{ij} + \hat{\sigma}_{ij}\hat{\sigma}_{kl} d_{kl}, \quad N_{ij} = a_1\left(\hat{\sigma}_{ij} + \hat{\sigma}^*_{ij}\right), \tag{14}$$

where

$$a_1^{-1} = c_1 + c_2\sqrt{\hat{\sigma}^*_{kl}\hat{\sigma}^*_{lk}}[1 + \cos(3\theta)], \tag{15}$$

$$\cos(3\theta) = -\frac{\sqrt{6}}{\left[\hat{\sigma}^*_{kl}\hat{\sigma}^*_{kl}\right]^{1.5}}\left(\hat{\sigma}^*_{kl}\hat{\sigma}^*_{lm}\hat{\sigma}^*_{mk}\right), \tag{16}$$

$$c_1 = \sqrt{\frac{3}{8}}\frac{(3 - \sin\phi_c)}{\sin\phi_c}, \quad c_2 = \frac{3}{8}\frac{(3 + \sin\phi_c)}{\sin\phi_c}. \tag{17}$$

ϕ_c is the critical angle of internal friction during stationary flow. θ denote the Lode angle; the angle on the deviatoric plane $\sigma_1 + \sigma_2 + \sigma_3 = 0$ between the stress vector and the axis σ_3 (σ_i is the principle stress vector), and σ^*_{ij} denote the deviatoric part of σ_{ij} In case of sand, the hypoplastic constitutive relation is approximately valid in the pressure range 1 kPa $< -\sigma_{kk}/3 <$ 1000 kPa. Below this, additional

capillary forces due to the air humidity and van der Waals forces may become important, and above it, grain crushing.

The constitutive relationship requires 7 material constants: e_{i0}, e_{d0}, e_{c0}, ϕ_c, h_s, n and α. The FE-analyses were carried out with the following material constants (for so-called Karlsruhe sand): $e_{i0} = 1.3$, $e_{d0} = 0.51$, $e_{c0} = 0.82$, $\phi_c = 30°$, $h_s = 190$ MPa, $n = 0.5$ and $\alpha = 0.3$ (Bauer 1996). The parameters h_s and n are estimated from a single oedometric compression test with an initially loose specimen (h_s reflects the slope of the curve in a semilogarithmic representation, and n its curvature). The constant α is found from a triaxial test with a dense specimen (it reflects the height and position of the peak value of the stress-strain curve). The angle ϕ_c is determined from the angle of repose or measured in a triaxial test with a loose specimen. The values of e_{i0}, e_{d0}, e_{c0} are obtained with conventional index tests ($e_{c0} \approx e_{max}$, $e_{d0} \approx e_{min}$, $e_{i0} \approx (1.1 - 1.5) e_{max}$). The mean grain diameter of sand is $d_{50} = 0.5$ mm.

A hypoplastic constitutive law cannot describe realistically shear localisation since it does not include a characteristic length. A characteristic length was taken into account by means of a non-local theory.

3. Non-Local Hypoplasticity

A non-local approach has been proposed for concrete (Bazant et al 1987, Bazant and Lin 1988, Pijaudier-Cabot 1995, Chen 1999, Akkermann 2000, Bobinski and Tejchman 2002, 2003) and for soils (Brinkgreve 1994, Schanz 1998, Marcher and Vermeer 2001, Maier 2002) to regularise a boundary value problem and to calculate localisation of deformation in the form of shear zones and cracks. It is based on spatial averaging of tensor or scalar state variables in a certain neighbourhood of a given point (Eringen 1981), i.e. material response at a point depends on the both state of its neighbourhood and on the state in the point itself. Thus, a characteristic length can be incorporated and softening can spread over material points. In contrast, in classical continuum mechanics, the principle of local action holds (i.e. the dependent variables in each material point depend only upon the values of the independent variables at the same point). To obtain a full regularisation effect according to both the mesh size and mesh inclination, it is sufficient to treat non-locally only one internal constitutive variable, e.g. equivalent plastic strain in an elasto-plastic formulation (Bazant and Lin 1988, Marcher and Vermeer 2001, Bobiński and Tejchman 2003) or modulus of the deformation rate in a hypoplastic approach (Maier 2002) whereas the other variables retain their local definitions.

The advantages of a non-local approach are: it is suitable for both shear and tension (decohesion) dominated applications and is easy to implement. The disadvantages are: long a computation time and a characteristic length is not directly related to the micro-structure of materials.

The presented hypoplastic FE-calculations were carried out separately with: a) a non-local modulus of the deformation rate d^*, b) non-local density factor f_d^* and c) non-local stiffness factor f_s^* (stresses, strains and other variables remained local). These three parameters are always positive and are affected by softening to different extent (Fig. 2).

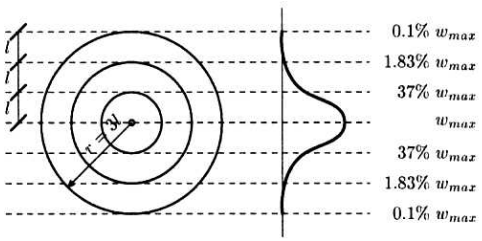

Fig. 1. Distribution of the weighting function w

In the first case, the modulus of the deformation rate (Eq. 6) expressed by

$$d = \sqrt{d_{kl} d_{kl}} \tag{18}$$

was treated non-locally:

$$d^*(x) = \frac{1}{A} \int_{-\infty}^{\infty} w(r) d(x + r) dV, \tag{19}$$

where r is the distance from the material point considered to other integration points of the entire material body, w is the weighting function and A is the weighted body volume. During a FE-analysis, all integrals were replaced by summation operators. Thus, Eq. 16 became:

$$d^*(x_i) = \frac{\sum_{j=1}^{np} w\left(|x_i - x_j|\right) d\left(x_j\right) A_j}{\sum_{j=1}^{np} w\left(|x_i - x_j|\right) A_j}, \tag{20}$$

where np is the number of all integration points in the whole body, x_j stands for co-ordinates of the integration point and A_j is the actual element area. The error density function (normal Gaussian distribution function) was chosen as a weighting function w (Brinkgreve 1994, Maier 2002):

$$w(r) = \frac{1}{l\sqrt{\pi}} e^{-\left(\frac{r}{l}\right)^2}. \tag{21}$$

The parameter l denotes a characteristic length (it determines the size of the neighbourhood influencing the state at a given point) and the parameter a is a weighting parameter. At the distance of a few times the length l, the function w is equal to zero (Fig. 1). Generally, the characteristic length l in Eq. 21 is not directly related to dimensions of the material microstructure, since it depends on the constitutive model and the weighting function.

In the second and third cases, the FE-calculations were carried out with a non-local density factor f_d^* and a non-local stiffness factor f_s^*, respectively, which were calculated with the aid of the local density factor f_d (Eq. 10) and the local stiffness factor f_s (Eq. 8) using Eqs. 19–21 (with $a = 1$).

4. FE-Implementation

FE-calculations of plane strain compression tests were performed with a sand specimen which was $h_o = 10$ cm high and $b = 2$ cm wide. Only quadrilateral finite elements composed of four diagonally crossed triangles were applied to avoid volumetric locking. In all, 320 quadrilateral elements (0.25×0.25 cm) divided into 1280 triangular elements with linear shape functions for displacements were used. The dimensions of finite elements were $5 \times d_{50}$ to obtain the thickness of shear zones irrespective of the mesh size (Tejchman et al 1999, Maier 2002). The integration was performed with one sampling point placed in the middle of each element. The calculations were carried out with slight deformations.

As the initial stress state, a K_0-state with $\sigma_{22} = \sigma_c + \gamma dx_2$ and $\sigma_{11} = \sigma_c + K_0 \gamma dx_2$ was assumed in the sand specimen where σ_c denotes the confining pressure, x_2 is the vertical coordinate measured from the top of the specimen, γd denotes the initial density and $K_0 = 0.45$ is the earth pressure coefficient at rest (σ_{11} – horizontal normal stress, σ_{22} – vertical normal stress).

A quasi-static deformation in sand was initiated through a constant vertical displacement increment prescribed at nodes along the upper edge of the specimen. The boundary conditions of the sand specimen were no shear stress at the top and bottom. To preserve the stability of the specimen against sliding along the bottom boundary, the node in the middle of the bottom was kept fixed. To obtain a shear zone inside the specimen (in the central part), a weaker element with a high initial void ratio, $e_0 = 0.90$, was inserted in the middle of the left side of the specimen.

For the solution of a non-linear system, a modified Newton-Raphson scheme with line search was used with a global stiffness matrix calculated with only the first term of the constitutive equations (linear in d_{kl}). The stiffness matrix was updated every 100 steps. To accelerate the calculations in the softening regime, the initial increments of displacements in each calculation step were assumed to be equal to the final increments in the previous step. The iteration steps were

performed using translational convergence criteria. For the time integration of stresses in finite elements, a one-step Euler forward scheme was applied.

The local model was implemented in the author's finite element code.

5. FE-Results

5.1. Local Continuum

Figures 2 and 3 present the results of plane strain compression with dense sand ($e_o = 0.60$) within a conventional (local) continuum (Eqs. 1–17) under confining pressure $\sigma_c = 0.2$ MPa. The normalized load-displacement curve is depicted in Fig. 2a. Figure 2b shows the deformed FE-mesh with the distribution of void ratio. The darker the regin, the higher the void ratio. The evolution of the void ratio e, density factor f_d (Eq. 10), stiffness factor f_s (Eq. 8), modulus of the deformation rate d (Eqs. 6) and Lode angle θ (Eq. 16) at two different locations: inside the shear zone and far beyond it are demonstrated in Fig. 3.

The resultant vertical force on the specimen top P increases first, shows a pronounced peak, drops later and reaches a residual state (Fig. 2a). The overall angle of internal friction for the sand specimen, calculated from Mohr's formula

$$\phi = \arcsin \frac{\sigma_1 - \sigma_2}{\sigma_1 + \sigma_2} \tag{22}$$

is equal to $\phi_p = 42.9°$ at peak ($u/h_0 = 2.4\%$). At residual state, it is equal to $\phi_{cr} = 32.2°$ ($u/h_0 = 4\%$) and different from the assumed critical angle of internal friction, $\phi_c = 30°$ (Eq. 17). In Eq. 22, $\sigma_1 = P/(bl)$ denotes the vertical principle stress ($\sigma_2 = \sigma_c$ is the horizontal principal stress, $b = 0.02$ m is the specimen width, $l = 1.0$ m and u denotes the vertical displacement of the top).

At the beginning of the compression process, two shear zones are created expanding outward from the weakest element. Afterwards, and up to the end, only one shear zone dominates. The complete shear zone is already noticeable shortly after the peak. It is characterised by both a concentration of shear deformations, and a significant increase of the void ratio and modulus of the deformation rate. The calculated thickness of the shear zone is equal to the width of finite elements and its inclination is equal to the mesh orientation.

The void ratio e at the beginning decreases (up to $u/h_0 = 1\%$) and afterwards increases in the whole specimen (Fig. 3a). In the shear zone, it reaches a pressure-dependent critical value at residual state ($e = e_c = 0.745$, Eq. 13). Beyond the shear zone, the void ratio reaches the initial value. The thickness of the shear zone on the basis of an increase of the void ratio is slightly larger since a dense granular material already dilates before a shear zone is created.

The density factor f_d (Eq. 10) continuously increases in the whole specimen (Fig. 3b). At residual state, it is equal to 1.0 (shear zone) and 0.8 (remaining region).

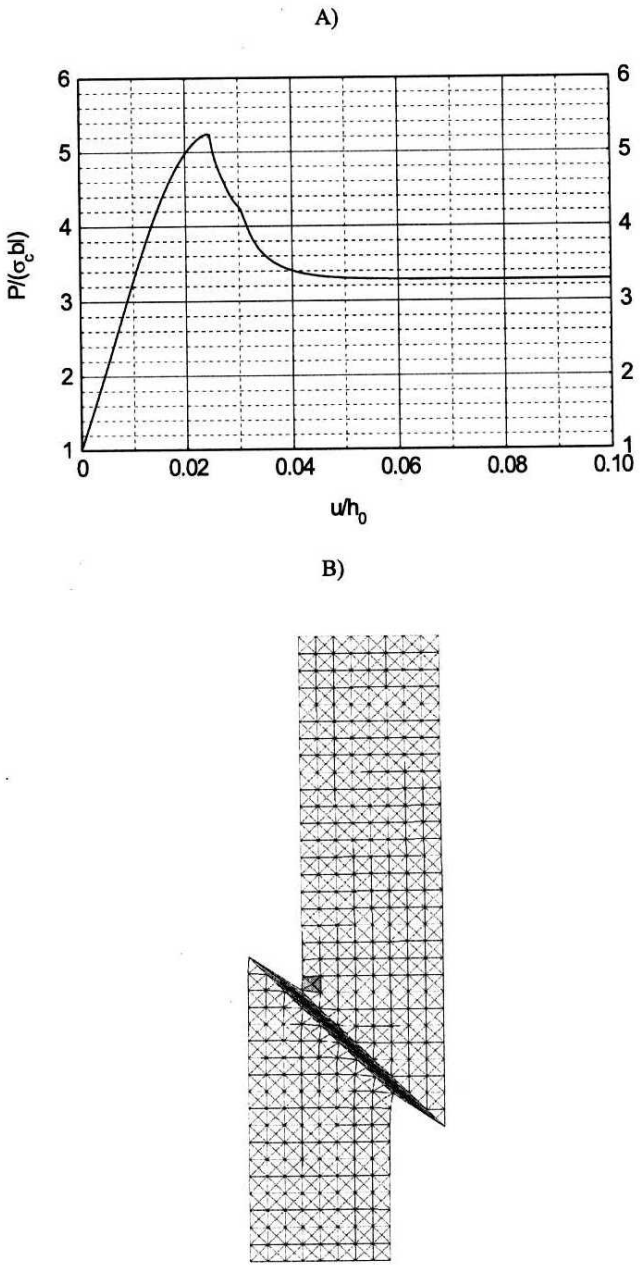

Fig. 2. Load-displacement curve and deformed FE-mesh with the distribution of void ratio in the residual state (local continuum, $e_o = 0.60$, $\sigma_c = 0.2$ MPa)

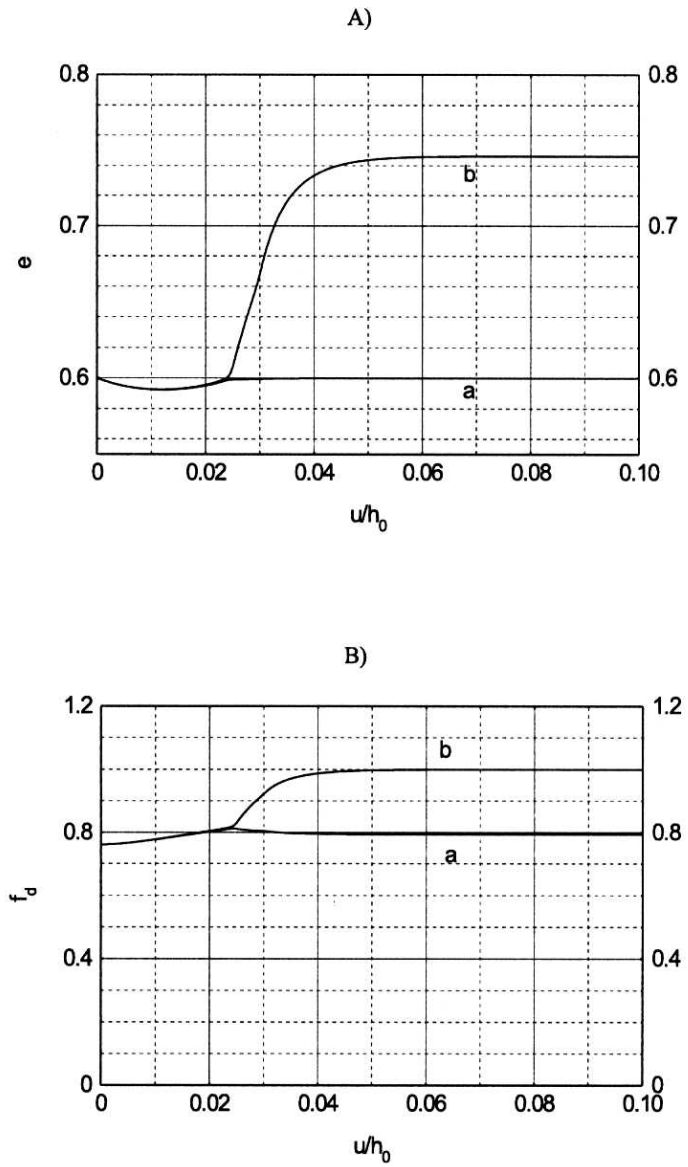

Fig. 3. Evolution of (A) void ratio e, (B) density factor f_d, (a – outside the shear zone, b – in the shear zone)

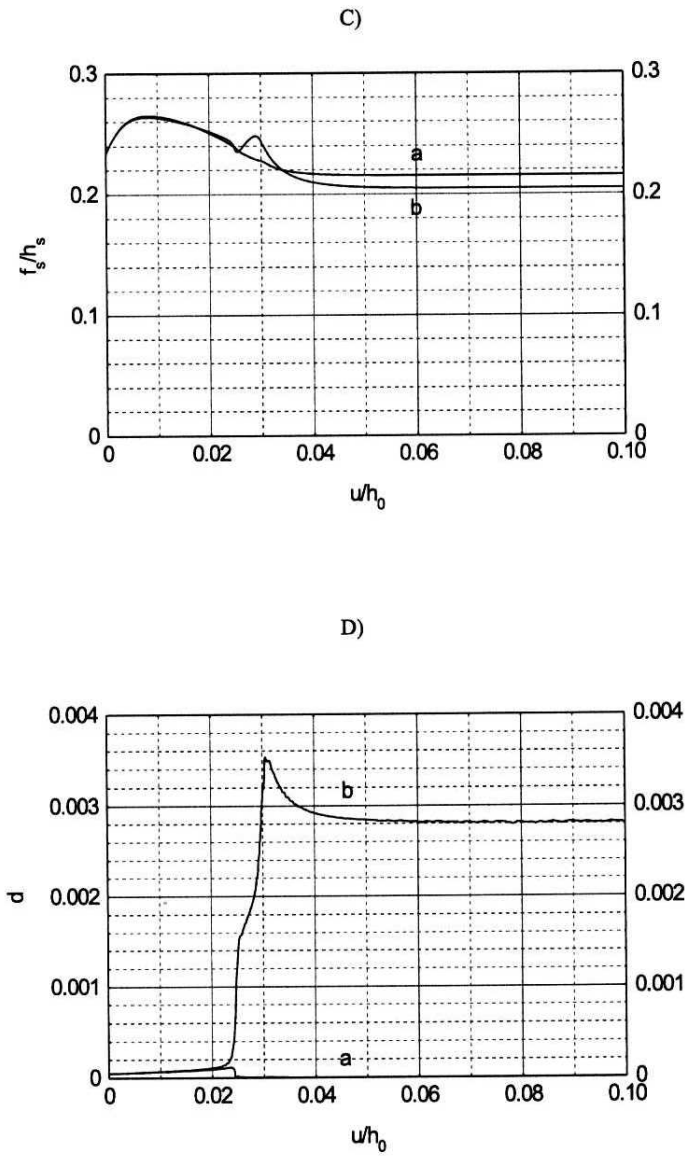

Fig. 3. Evolution of (C) normalized stiffness factor f_s/h_s, (D) modulus of the deformation rate d (a – outside the shear zone, b – in the shear zone)

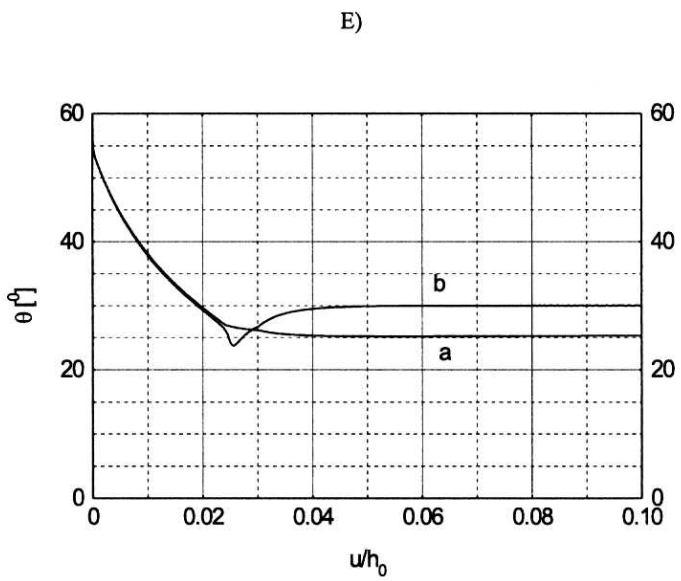

Fig. 3. Evolution of (E) Lode angle θ (a – outside the shear zone, b – in the shear zone)

Outside the shear zone, the normalized stiffness factor f_s/h_s increases up to $u/h_0 = 0.5\%$, then decreases reaching an asymptote at $u/h_0 = 4\%$. In the shear zone, the stiffness factor increases up to $u/h_0 = 0.5\%$, then decreases up to $u/h_0 = 2.4\%$. At the peak of the resultant vertical force on the top, it increases again, then decreases later reaching an asymptote. At residual state, it is smaller by 10% as compared with the value beyond the shear zone.

The modulus of the deformation rate d increases uniformly throughout the whole specimen from the beginning of loading up to $u/h_0 = 2\%$. Later, it is significant only in the shear zone (Fig. 3d). It increases substantially in the range of $u/h_0 = 2$–3%. Afterwards, it decreases and approaches an asymptote. On the basis of the difference between the modulus of the deformation rate in the shear zone and beyond it, one can find that the shear zone is created before the peak of the resultant vertical force on the top, namely at $u/h_0 = 2\%$.

The Lode angle θ (Eq. 13) is equal to 30° in the shear zone and 25° beyond this (residual state).

5.2. Non-Local Continuum

The results with a non-local modulus of the deformation rate d^* using a different characteristic length l of Eq. 21 (0.5 mm, 1.0 mm and 2.0 mm) with the weighting parameter a =1 of Eq. 21 and dense sand ($e_o = 0.60$, $\sigma_c = 0.2$ MPa) are shown in Fig. 4. The effect of the weighting factor a is depicted in Fig. 5. In turn, Figure 6

demonstrates the effect of the initial void ratio and pressure level on results with $a = 0.5$.

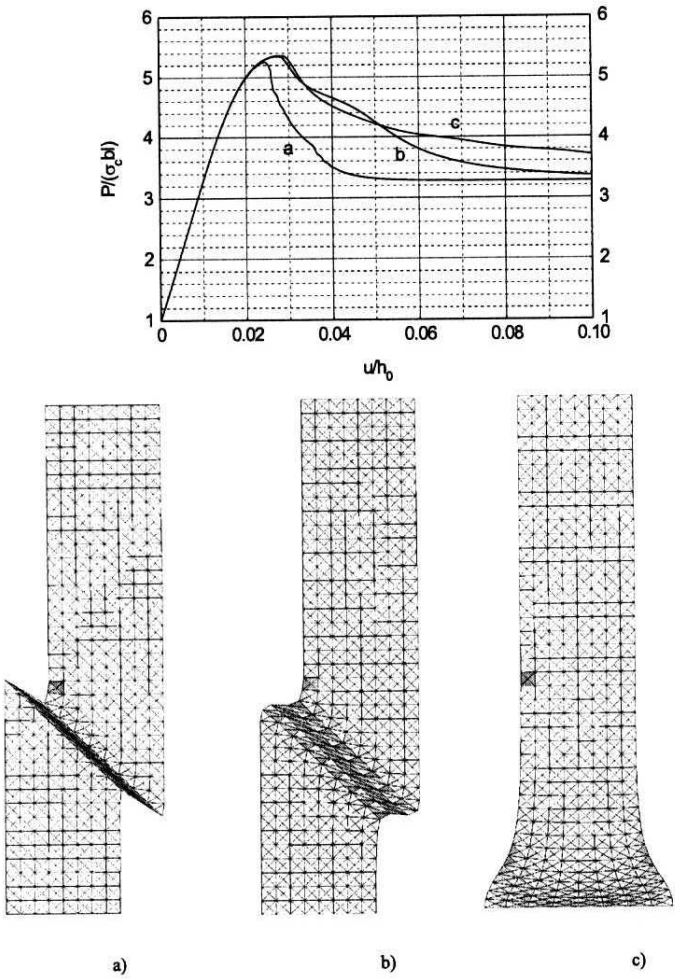

Fig. 4. Load-displacement curves and deformed FE-meshes with the distribution of void ratio in the residual state (non-local continuum, $e_o = 0.60$, $\sigma_c = 0.2$ MPa, $a = 1.0$): a) $l = 0.5$ mm, b) $l = 1.0$ mm, c) $l = 2$ mm

The larger the characteristic length, the greater both the maximum and residual vertical force on the top, the smaller the material softening and the greater the vertical displacement of the top corresponding to the peak and residual force (Fig. 4). Thus, the forces and corresponding vertical displacements are higher than within a non-local continuum. The mean angles of internal friction for the entire sand specimen are equal to $\phi_p = 43.3°$–$42.9°$ (peak) and $\phi_{cr} = 35.1°$–$32.2°$ (residual state). The obtained results of internal friction angles at peak and in the

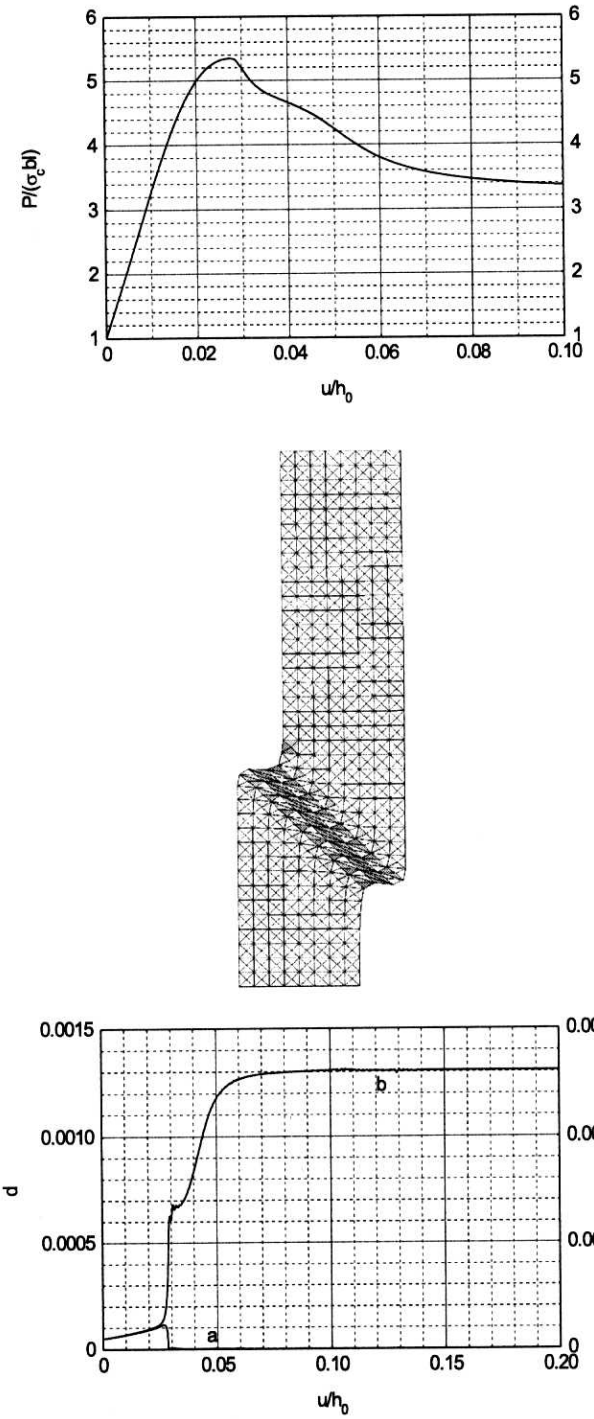

Fig. 5. Load-displacement curve, deformed FE-mesh with the distribution of void ratio in the residual state and evolution of modulus of the deformation rate d (non-local continuum, $l = 0.5$ mm, $e_o = 0.60$, $\sigma_c = 0.2$ MPa, $a = 0.5$): a – outside the shear zone, b – in the shear zone

residual state in dense sand, and the corresponding vertical displacements of the sand specimen compare well with experimental results with Karlsruhe sand carried out by Vardoulakis (1977, 1980) and Yoshida et al. (1994). In the experiments by Vardoulakis (1977, 1980), the dimensions of the specimen were: $h_0 = 140$ mm, $b = 40$ mm, $l = 80$ mm, and in the experiments by Yoshida et al (1994): $h_0 = 200$ mm, $b = 80$ mm, $l = 160$ mm, respectively. The experiments with very dense sand ($e_o = 0.55$) resulted in $\phi_p = 45.7^o$ and $\phi_{cr} = 32.9^\circ$ (Vardoulakis 1977, 1980), and $\phi_p = 43.4^o$, and $\phi_{cr} = 31.3^\circ$ (Yoshida et al 1994) at $\sigma_c = 200$ kPa. However, the shape of the calculated load-displacement curves differs slightly. Contrary to the experiments, the calculated stiffness is too small at the beginning of the loading process and too high close to the peak of the load-displacement curve (in the hardening and softening regime).

The thickness of the shear zone increases with increasing characteristic length. The thickness of the internal shear zone is: $t_{sz} \cong 3 \times l$ ($l = 0.5$ mm) and $t_{sz} \cong 7 \times l$ ($l = 1.0$ mm). If the characteristic length is greater ($l = 2.0$ mm), the shear zone does not appear (the deformations are concentrated at the bottom of the specimen). The calculated thickness of the shear zone in dense Karlsruhe sand with $l = 1$ mm is in accordance with the observed thickness during experiments at $\sigma_c = 200$ kPa: $t_{sz} = 13 \times d_{50}$ (Vardoulakis 1977, 1980) and $10 \times d_{50}$ (Yoshida et al 1994), if one assumes that the non-local characteristic length is $l \cong 2 \times d_{50}$. This result is also in agreement with FE-calculations carried out by Maier (2002).

In turn, the results of t_{sz} with $l = 0.5$ mm and $a = 0.5$ of Eq. 21 (Fig. 5) are similar to those with $l = 1.0$ mm and $a = 1.0$ ($t_{sz} \cong 14 \times l$). Thus, the non-local characteristic length can be directly related to the mean grain diameter ($l \cong d_{50}$) by a modification of the weighting function w (Eq. 21). On the basis of the difference between the modulus of deformation in the shear zone and beyond it at the beginning of loading (Fig. 5c), one can deduce that the shear zone is created slightly before the peak of the vertical force on the top at $u/h_0 = 2.5\%$.

In the case of a higher initial void ratio e_0 and higher lateral pressure σ_c, the thickness of the internal shear zone ($l = 0.5$ mm, $a = 0.5$) is: $t_{sz} \cong 20 \times l$ ($e_0 = 0.70$, $\sigma_c = 0.2$ MPa) and $t_{sz} \cong 16 \times l$ ($e_0 = 0.60$, $\sigma_c = 0.5$ MPa), Fig. 6. Thus, the numerical results demonstrate that the higher the initial void ratio and confining pressure, the lower the maximum normalized vertical force on the top. The higher the initial void ratio and confining pressure, the smaller the material softening. With an increase of the initial void ratio and confining pressure, the vertical displacement related to the peak force P becomes larger. An increase of the thickness of the shear zone with increasing e_0 and σ_c corresponds to a decrease of the rate of softening. The material becomes softer, and thus a larger deformation can develop (Tejchman et al 1999).

The distribution of void ratio in the shear zone is slightly non-uniform.

If the density factor f_d of Eq. 10 is treated non-locally ($a = 1.0$), a regularisation effect appears for a considerably greater characteristic length ($l \geq 10$ mm),

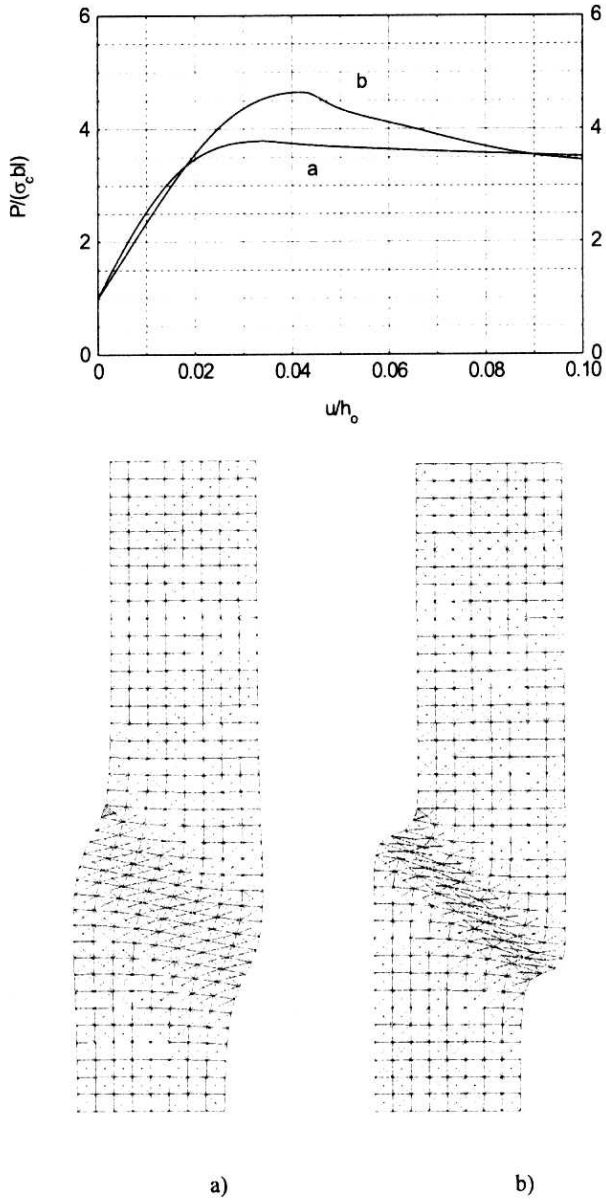

Fig. 6. Load-displacement curves and deformed FE-meshes with the distribution of void ratio in the residual state (non-local continuum, $a = 0.5$, $l = 0.5$ mm):
a) $e_o = 0.70$, $\sigma_c = 0.2$ MPa, b) $e_o = 0.60$, $\sigma_c = 0.5$ MPa

Fig. 7. The non-local results with $l = 20$ mm correspond approximately to the results with a non-local modulus of the deformation rate at ($l = 1.0$ mm) (Fig. 4). The distribution of the void ratio is more uniform as compared with results with a non-local modulus of the deformation rate (Fig. 4).

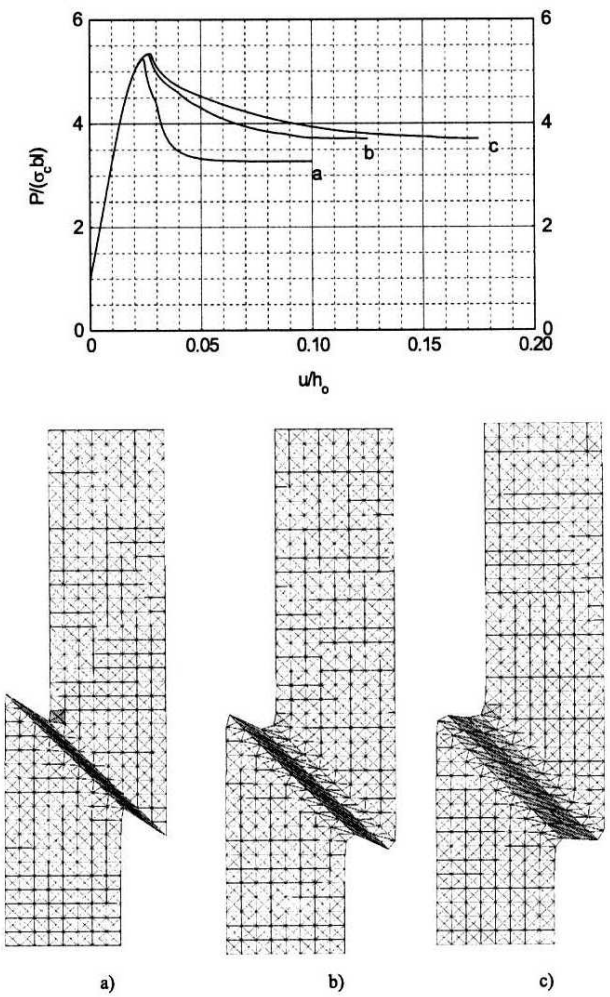

Fig. 7. Load-displacement curves and deformed FE-meshes with the distribution of void ratio in the residual state (non-local density factor, $a = 1.0$, $e_o = 0.60$, $\sigma_c = 0.2$ MPa,): a) $l = 1.0$ mm, b) $l = 10.0$ mm, c) $l = 20.0$ mm

In the case of a non-local stiffness factor f_s of Eq. 8, a regularisation effect did not occur even at l =100 mm (due to a small difference between the values in the shear zone and outside it, Fig. 3c).

6. Conclusions

The FE-calculations of a plane strain compression test for granular materials demonstrate that a local hypoplastic constitutive model suffers from mesh-dependency. The thickness of shear zones inside a specimen and load-displacement diagrams are severely mesh-dependent.

A non-local hypoplastic model provides full regularisation of the boundary value problem during plane strain compression. Numerical solutions converge to a finite size of the localisation zone upon mesh refinement.

The thickness of a localised shear zone increases with increasing characteristic length, confining pressure, and initial void ratio.

The characteristic length in a non-local continuum can be directly related to a mean grain diameter of the granular material by modification of the weighting function.

The thickness of a shear zone greatly depends on the choice of the non-local internal constitutive variable. The non-local modulus of the deformation rate has the strongest regularisation effect.

Increasing void ratio and modulus of the deformation rate are good indicators for shear zones.

A characteristic length of a non-local model can be calibrated for different sands with a numerical analysis of a plane strain compression test.

The FE-studies on shear localisation in granular bodies will be continued. A hypoplastic constitutive law will be extended by a strain gradient approach and compared with a polar (Tejchman et al 1999, Tejchman 2002) and non-local approach. In this enhanced hypoplastic model, a characteristic length will be incorporated with the aid of gradients of different internal constitutive variables (Voyiadjis and Dorgan 2003).

References

Akkermann J. (2000), *Rotationsverhalten von Stahlbeton-Rahmennecken*, Dissertation, Universitat Fridericiana zu Karlsruhe, Karlsruhe.

Bauer E. (1996), Calibration of a Comprehensive Hypoplastic Model for Granular Materials, *Soils and Foundations*, 36, 1, 13–26 .

Bazant Z., Lin Z., Pijaudier-Cabot F. G. (1987), Yield Limit Degradation: Non-Local Continuum Model with Local Strain. *Proc. Int. Conf. Computational Plasticity, Barcelona*, 1757–1780.

Bazant Z. P., Lin F. (1988), Non-Local Yield Limit Degradation, *Int. J. Num. Meth. Engng.* 35, 1805–1823.

Belytschko T., Chiang H., Plaskacz E. (1994), High Resolution Two Dimensional Shear Band Computations: Imperfections and Mesh Dependence, *Com. Meth. Appl. Mech. Engng.*, 119, 1–15.

Benallal A., Billardon R., Geymonat G. (1987), Localization Phenomena at the Boundaries and Interfaces of Solids, *Proc. of the 3rd Int. Conf. Constitutive Laws for Engineering Materials: Theory and Applications*, Tucson, Arizona, 387–390.

Bobinski J., Tejchman J. (2002), A Non-Local Elasto-Plastic Model to Describe Localisations of Deformation in Concrete, *Task Quarterly*, Gdańsk, 6, 3, 427–437 .

Bobinski J., Tejchman J. (2003), A Non-Local Elasto-Plastic Model to Simulate Localizations of Deformations in Quasi-Brittle Materials, *Proc. 15th Intern. Conference on Computer Mechanics CMM-2003*, 1–6.

Borst R. de, Mühlhaus H.-B., Pamin J., Sluys L. (1992), Computational Modelling of Localization of Deformation, *Proc. of the 3rd Int. Conf. Comp. Plasticity*, Swansea, 483–508, Pineridge Press.

Brinkgreve R. (1994), Geomaterial Models and Numerical Analysis of Softening, *Dissertation*, Delft University, 1–153.

Chambon R., Matsushima T., Caillerie D. (2001), Plastic Continuum with Microstructure, Local Second Gradient Theories for Geomaterials: Localisation Studies, *Int. Journal of Solids and Structures*, 38, 8503–8527.

Chen E. P. (1999), Non–Local Effects on Dynamic Damage Accumulation in Brittle Solids, *I. J. Num. Anal. Meth. Geomech.* 23, 1–21.

Desrues J., Chambon R., Mokni M., Mazerolle F. (1996), Void Ratio Evolution Inside Shear Bands in Triaxial Sand Specimens Studied by Computed Tomography, *Géotechnique*, 46, 3, 529–546.

Ehlers W., Volk W. (1998), Fundamental Considerations on the Numerical Investigation of Shear Band Phenomena in Saturated and Non-Saturated Frictional Porous Materials, [in:] *Computational Mechanics – New Trends and Applications*, S. Idelsohn, E. Onate, E. Dworkin, editors, CIMNE Barcelona, 1–20.

Eringen A. C. (1981), On Non-Local Plasticity, *Int. J. Engineering Science*, 19, 1461–1474.

Gudehus, G. (1996), A Comprehensive Constitutive Equation for Granular Materials, *Soils and Foundations*, 36, 1, 1–12.

Hassan A. H. (1995), Etude Experimentale et Numerique du Comportement Local et Global d'une Interface Sol Granulaire Structure, *Dissertation*, Grenoble University.

Herle I., Gudehus G. (1999), Determination of Parameters of a Hypoplastic Constitutive Model from Grain Properties, *Mechanics of Cohesive-Frictional Materials*, 4, 5, 461–486.

Maier T. (2002), Numerische Modellierung der Entfestigung im Rahmen der Hypoplastizität, *PhD Thesis*, University of Dortmund.

Marcher T., Vermeer P.A. (2001), Macro-Modelling of Softening in Non-Cohesive Soils, [in:] *Continuous and Discontinuous Modelling of Cohesive-Frictional Materials*, P. A. Vermeer et al, editors, Springer–Verlag, 89–110.

Mühlhaus H. B. (1990), Continuum Models for Layered and Blocky Rock, [in:] *Comprehensive Rock Engineering*, J. A. Hudson, Ch. Fairhurst, editors, 2, 209–231, Pergamon Press.

Neddleman A. (1988), Material Rate Dependence and Mesh Sensitivity in Localization Problems, *Comp. Meths. Appl. Mech. Eng.*, 67, 69–85.

Needleman A., Tvergaard V. (1992), Analyses of Plastic Flow Localization in Metals, *Applied Mechanics Reviews*, 45, 3, 2–18.

Pijaudier-Cabot G. (1995), Non Local Damage, [in:] *Continuum Models for Materials with Microstructure*, H. B. Mühlhaus, editor, John Wiley & Sons Ltd.

Schanz T. (1998), A Constitutive Model for Cemented Sands, [in:] *Localisation and Bifurcation Theory for Soils and Rocks*, Adachi, Oka, Yashima, editors, Balkema, Rotterdam, 165–172.

Sluys L. Y. (1992), Wave Propagation, Localisation and Dispersion in Softening Solids, *PhD Thesis*, Delft University of Technology.

Tatsuoka F., Okahara M., Tanaka T., Tani K., Morimoto T., Siddiquee M. S. (1991), Progressive Failure and Particle Size Effect in Bearing Capacity of Footing on Sand, *Proc. of the ASCE Geotechnical Engineering Congress*, 27, 2, 788–802.

Tatsuoka F., Siddiquee M. S., Yoshida T., Park C. S., Kamegai Y., Goto S., Kohata Y. (1994), *Testing Methods and Results of Element Tests and Testing Conditions of Plane Strain Model Bearing Capacity Tests using Air-Dried Dense Silver Buzzard Sand*, Internal Report, University of Tokyo, 1–129.

Tejchman J. (1989), Scherzonenbildung und Verspannungseffekte in Granulaten unter Berücksichtigung von Korndrehungen, *Publication Series of the Institute of Soil and Rock Mechanics, University Karlsruhe*, 117, 1–236.

Tejchman J., Wu W. (1993), Numerical Study on Shear Band Patterning in a Cosserat Continuum, *Acta Mechanica*, 99, 61–74.

Tejchman J. (1997), *Modelling of Shear Localisation and Autogeneous Dynamic Effects in Granular Bodies*, Publication Series of the Institute for Soil and Rock Mechanics, University Karlsruhe, 140.

Tejchman J., Herle I., Wehr J. (1999), FE-studies on the Influence of Initial Void Ratio, Pressure Level and Mean Grain Diameter on Shear Localization, *Int. J. Num. Anal. Meth. Geomech.*, 23, 15, 2045–2074.

Tejchman J. (2002), Patterns of Shear Zones in Granular Materials within a Polar Hypoplastic Continuum, *Acta Mechanica*, 155, 1–2, 71–95.

Uesugi M., Kishida H., Tsubakihara Y. (1988), Behaviour of Sand Particles in Sand-Steel Friction, *Soils and Foundations*, 28, 1, 107–118.

Vardoulakis I. (1977), *Scherfugenbildung in Sandkörpern als Verzweigungsproblem*, Dissertation, Institute for Soil and Rock Mechanics, University of Karlsruhe, 70.

Vardoulakis I. (1980) Shear Band Inclination and Shear Modulus in Biaxial Tests, *Int. J. Num. Anal. Meth. Geomech.*, 4, 103–119.

Voyiadjis G. Z., Dorgan R. (2003), Gradient Dependent Computational Models for Localization Problems in Materials, *Proc. CMM-2003*, Gliwice, Poland, 1–10.

Wang C. C. (1970), A New Representation Theorem for Isotropic Functions, *J. Rat. Mech. Anal.*, 36, 166–223.

von Wolffersdorff P. A. (1996), A Hypoplastic Relation for Granular Materials with a Predefined Limit State Surface, *Mechanics Cohesive-Frictional Materials*, 1, 251–271.

Wu W., Niemunis A. (1996), Failure Criterion, Flow Rule and Dissipation Function Derived from Hypoplasticity, *Mechanics of Cohesive-Frictional Materials*, 1, 145–163.

Zbib H. M., Aifantis E. C. (1988), On the Localisation and Postlocalisation Behaviour of Plastic Deformation, *Res Mechanica* 23, 261–277.

Yoshida T., Tatsuoka F., Siddiquee M. (1994), Shear Banding in Sands observed in Plane Strain Compression, [in:] *Localisation and Bifurcation Theory for Soils and Rocks*, R. Chambon, J. Desrues and I. Vardoulakis, editors, 165–181, Balkema, Rotterdam.

Yagi K., Miura S., Asonuma T., Sakon T., Nakata T. (1997), Particle Crushing and Shear Banding of Volcanic Coarse-Grained Soils, [in:] *Deformation and Progressive Failure in Geomechanics*, A. Asaoka, T. Adachi, F. Oka, editors, 139–145, Pergamon.